ResearchGate

See discussions, stats, and author profiles for this publication at: https://www.researchgate.net/publication/290443952

# Connecting Active-Site Loop Conformations and Catalysis in Triosephosphate Isomerase: Insights from a Rare Variation at Residue 96 in the Plasmodial Enzyme

**Article** *in* ChemBioChem · January 2016

DOI: 10.1002/cbic.201500532

CITATIONS
10

READS
87

**6 authors**, including:

Vidhi Pareek
Pennsylvania State University
**9** PUBLICATIONS **224** CITATIONS
SEE PROFILE

niranjan.v. Joshi
Indian Institute of Science
**122** PUBLICATIONS **3,003** CITATIONS
SEE PROFILE

Mathur R N Murthy
Indian Institute of Science
**188** PUBLICATIONS **3,661** CITATIONS
SEE PROFILE

Padmanabhan Balaram
Indian Institute of Science
**595** PUBLICATIONS **19,813** CITATIONS
SEE PROFILE

**Some of the authors of this publication are also working on these related projects:**



Bioactive peptides View project



Integrated Ecological Carrying Capacity of Uttara Kannada, Karnataka View project

All content following this page was uploaded by Vidhi Pareek on 28 September 2021.

The user has requested enhancement of the downloaded file.

ChemPubSoc Europe

DOI: 10.1002/cbic.201500532

CHEMBIOCHEM Full Papers

# Connecting Active-Site Loop Conformations and Catalysis in Triosephosphate Isomerase: Insights from a Rare Variation at Residue 96 in the Plasmodial Enzyme

Vidhi Pareek,[a] Moumita Samanta,[a] Niranjan V Joshi,[b] Hemalatha Balaram,[c] Mathur R. N. Murthy,[a] and Padmanabhan Balaram*[a]

Despite extensive research into triosephosphate isomerases (TIMs), there exists a gap in understanding of the remarkable conjunction between catalytic loop-6 (residues 166–176) movement and the conformational flip of Glu165 (catalytic base) upon substrate binding that primes the active site for efficient catalysis. The overwhelming occurrence of serine at position 96 (98% of the 6277 unique TIM sequences), spatially proximal to E165 and the loop-6 residues, raises questions about its role in catalysis. Notably, *Plasmodium falciparum* TIM has an extremely rare residue—phenylalanine—at this position whereas, curiously, the mutant F96S was catalytically defective. We have obtained insights into the influence of residue 96 on the loop-6 conformational flip and E165 positioning by combining kinetic and structural studies on the PfTIM F96 mutants F96Y, F96A, F96S/S73A, and F96S/L167V with sequence conservation analysis and comparative analysis of the available apo and holo structures of the enzyme from diverse organisms.

## Introduction

The growing body of enzyme sequences derived by genome sequencing projects can provide valuable insights into the nature of mutational variations in the vicinity of the active site. Whereas residues directly involved in catalytic steps are largely conserved, proximal residues can be varied, with evolutionary selection pressure allowing for compensatory mutations. The observation of a very rare mutational variant at residue 96 in the triosephosphate isomerase (TIM or TPI, EC 5.3.1.1) of the malarial parasite *Plasmodium falciparum* (Pf) permits investigation of the connection between the active-site loop-6 conformational flip and the catalytic residues.

TIM, a highly proficient ubiquitous enzyme, catalyzes interconversion of the two glycolytic intermediates—dihydroxyacetone phosphate (DHAP) and D-glyceraldehyde-3-phosphate (D-GAP)—$10^9$ times faster than the uncatalyzed reaction.[1–3] Systematic kinetic, mutational, and structural studies have revealed that abstraction of the C1/C2 proton of the substrate by the catalytic base E165 initiates the reaction, followed by a relay of proton-transfer steps involving residues K12, H95, and E97 (Figure S1 in the Supporting Information).[4–11] TIM achieves high catalytic efficiency through precise positioning of the catalytic residues[12] and a controlled and coordinated movement of the catalytic loop-6[13,14] (consensus-166-PVWAIGTGKTA-176, numbering as PfTIM; Figure S2) and the loop-7.[15,16] Loop-6 closure over the active site (the tip of the loop, Gly171, undergoes a displacement of 7 Å between loop-*closed* and -*open* states)[12,13] in conjunction with substrate binding leads to: 1) stabilization of the substrate and the intermediate through the formation of a hydrogen bond between the phosphodianion group of the substrate and the backbone –NH group of G171,[17] 2) expulsion of the bulk water from the active site (this allows efficient isomerization by internal proton transfer and alleviates the competing phosphate elimination reaction, which leads to the formation of the toxic metabolite methylglyoxal),[14,18–22] and 3) orientation of the E165 side chain carboxylate group proximal to the substrate (2 Å movement of the E165 side chain carboxylate group transiting from the "swung-out" to the catalytically competent "swung-in" conformation (Figure S2),[12] thus allowing efficient proton abstraction from the carbon backbone of the substrate. At the end of the catalytic cycle, loop opening permits product release.[23] Solution- and solid-state NMR and fluorescence spectroscopy studies have shown the loop-6 dynamics to be partially rate-limiting.[23,24] The human TIM loop-6 mutation I170V causes neurologic disorders and is of specific relevance in the context of this study.[25]

Over a quarter of a century ago, with a limited number of TIM sequences available, Ser96 appeared to be a fully conserved residue (Table 1, Figures 1A and S3). However, there was no evidence for its direct participation in catalysis. This observation led Alber et al. to remark that "the role of the conserved serine 96 is a mystery".[26] Indeed, in the large number

[a] V. Pareek, Dr. M. Samanta, Prof. M. R. N. Murthy, Prof. P. Balaram
Molecular Biophysics Unit, Indian Institute of Science
Bangalore 560012 (India)
E-mail: pb@mbu.iisc.ernet.in

[b] Prof. N. V. Joshi
Centre for Ecological Sciences, Indian Institute of Science
Bangalore 560012 (India)

[c] Prof. H. Balaram
Molecular Biology and Genetics Unit
Jawaharlal Nehru Centre for Advanced Scientific Research
Jakkur, Bangalore 560064 (India)

Supporting information for this article is available on the WWW under http://dx.doi.org/10.1002/cbic.201500532.


© 2016 Wiley-VCH Verlag GmbH & Co. KGaA, Weinheim

**Table 1.** Natural variation observed at positions 96, 73, 167, and 170 in the curated dataset of 6277 unique TIM sequences.

| Organism[a] | Position ($\eta$)[b] | Residue variability and occurrence frequency[c] | | | | |
|---|---|---|---|---|---|---|
| bacteria (5216) | 96 (10) | S 5140 | A 35 | I 16 | L 12 | C 5 |
| | 73 (9) | A 4994 | P 114 | S 60 | Q 26 | G 7 |
| | 167 (15) | V 2802 | I 2274 | S 57 | L 34 | E 11 |
| | 170 (3) | I 5143 | V 70 | M 3 | | |
| eukaryotes (819) | 96 (3) | S 802 | F 12 | A 5 | | |
| | 73 (5) | A 793 | S 13 | P 10 | D 2 | Q 1 |
| | 167 (4) | V 682 | I 132 | L 4 | M 1 | |
| | 170 (2) | V 818 | V 1 | | | |
| archaea (242) | 96 (1) | S 242 | | | | |
| | 73 (6) | S 165 | A 56 | G 17 | P 2 | Q 1 |
| | 167 (2) | P 240 | V 2 | | | |
| | 170 (1) | I 242 | | | | |

[a] Number of unique TIM sequences in each organism subset. [b] $\eta$ is the total number of different amino acids observed at a position. [c] Five most frequently occurring amino acids with associated frequencies observed in decreasing order.

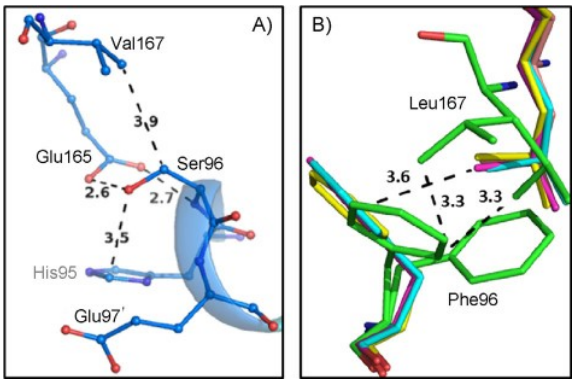


**Figure 1.** A) Residue 96 (serine in yeast TIM, PDB ID: 1YPI) interactions with E165 side chain (hydrogen bond with the backbone amide –NH group and side chain –OH group) and residue 167 side chain (van der Waals contact). B) Structural flexibility and correlated movement of residue 96 and 167 side chains is evident. Overlay of WT PfTIM- PDB ID: 1LYX (green), 1LZO (yellow), 1O5X (cyan), 1M7O (magenta), 1M7P (light pink).

of TIM sequences that have become available subsequently, the strong preference for serine at this position is retained and is striking (Table 1). Zhang et al. have suggested a role for Ser96 in positioning critical water molecules in the active site.[27]

A remarkable feature of TIM from all *Plasmodium* spp. is the presence of phenylalanine at this position (Figures 1B and S2C, Tables S1 and S3). Curiously, the replacement of F96 with serine in *Pf*TIM reduced the activity drastically (~300-fold drop in $k_{cat}/K_m$ for F96S) and affected ligand binding properties (Table S4).[28] These observations suggest that the presence of phenylalanine at position 96 of all the plasmodial sequences might be the result of specific selective pressure relating to the role of residue 96 in catalysis.

Despite its unique position and high degree of conservation, the role of residue 96 has remained unclear. Rationally driven site-directed mutagenesis, based on PfTIM as the model, provided insights into the factors accounting for the overwhelming presence of serine at this position, as well as the exceptional case of the occurrence of phenylalanine in this position in the plasmodial sequences.

## Results

### Analysis of amino acid conservation at position 96

A crucial structural and/or functional role of an amino acid residue in an enzyme results in it showing a high degree of conservation, countering random mutations that arise during the course of evolution. On this premise, the observation that residue 96 is serine in 6178 (Table 1) out of 6277 protein sequences (curated dataset of unique TIM sequences, Table S2) is striking and is suggestive of strong functional selection acting on it. Residue 96 is a part of a highly conserved hexapeptide helical segment GHSERR (residue $^{94}$GHFERR$^{99}$, in PfTIM) (Figures 1 and S2). In the bacterial dataset of 5216 unique sequences—including reviewed (SWISS-PROT) and unreviewed sequences (TrEMBL) taken from the UniProt database—residue 96 is serine in an overwhelming 5134 sequences. Alanine (35), isoleucine (16), and leucine (12) are observed in a limited number of cases, whereas phenylalanine [five, *Enterococcus phoeniculicola* (R3TNL9), *Enterococcus malodoratus* (R2QYI4), *Serratia symbiotica str. "Cinaracedri"* (R4I1M7), *Mycoplasma* sp. CAG: 877 (R5LIN8), and *Candidatus Baumannia cicadellinicola* (A0A088N143)], tyrosine (four), glutamine (two), asparagine (two), and valine (one) are found as rare variations. Variability in the eukaryotic and archaeal datasets is even more limited (Table 1). The 12 eukaryotic sequences with phenylalanine at position 96 correspond to the 12 reported *Plasmodium* spp. sequences (Table S1). Inspection of the TIM gene sequences revealed that all the six serine codons (CGU, CGC, CGA, CGG, UCU, and UCC) are observed in substantial numbers for this position (data not shown). Two of these codons (UCU and UCC) can change into the phenylalanine codons (UUU and UUC; UUU observed for all plasmodial sequences) through a single base substitution. This raises a number of questions. Why is serine so highly favored at position 96? Can we explain the presence of phenylalanine at this position for the plasmodial sequences, and thus the loss of activity observed for F96 mutants of PfTIM? If we understand the role of residue 96 in TIM catalysis, can we engineer a revertant to rescue the defect in catalysis observed for F96S?

### Kinetic and structural investigations of the single-point mutants F96Y and F96A

To dissect the role of polarity versus size contribution of Phe96 in PfTIM, the two single-point mutants F96Y and F96A were engineered. Kinetic parameters for the mutants were determined by monitoring the conversion of GAP into DHAP by the coupled enzyme assay at 25 °C. The specificity coefficients ($k_{cat}/K_m$)


© 2016 Wiley-VCH Verlag GmbH & Co. KGaA, Weinheim

of the mutants F96Y ($k_{cat} \approx 55\ s^{-1}$, $K_m \approx 1.8$ mM, $k_{cat}/K_m \approx 30\ mM^{-1}\ s^{-1}$) and F96A ($k_{cat} \approx 380\ s^{-1}$, $K_m \approx 0.9$ mM, $k_{cat}/K_m \approx 440\ mM^{-1}\ s^{-1}$) were 400 and 27 times lower, respectively, than those of PfTIM WT ($k_{cat} \approx 4200\ s^{-1}$, $K_m \approx 0.35$ mM, $k_{cat}/K_m \approx 12000\ mM^{-1}\ s^{-1}$; Table 2).

**Table 2.** Kinetic parameters for PfTIM residue 96 mutants and WT.

| Enzyme | $k_{cat}$ [$s^{-1}$] | $K_m$ [mM] | $k_{cat}/K_m$ [$mM^{-1}\ s^{-1}$] |
|---|---|---|---|
| PfTIM WT | $4.3 \pm 0.3 \times 10^3$ | $0.35 \pm 0.05$ | $1.2 \times 10^4$ |
| F96S[28] | $6.2 \pm 0.2 \times 10$ | $2.20 \pm 0.03$ | $2.8 \times 10$ |
| F96Y | $5.5 \pm 0.2 \times 10$ | $1.85 \pm .08$ | $3.0 \times 10$ |
| F96A | $3.8 \pm 0.1 \times 10^2$ | $0.87 \pm .05$ | $4.4 \times 10^2$ |
| F96S/S73A | $4.6 \pm 0.1 \times 10$ | $1.20 \pm 0.10$ | $3.8 \times 10$ |
| F96S/L167V | $4.0 \pm 0.1 \times 10^2$ | $1.02 \pm 0.07$ | $3.9 \times 10^2$ |

It is apparent that the polar aromatic side chain of the Tyr residue is not suitable for efficient catalysis. In comparison, the small, nonpolar alanine residue is functionally more suitable. However, the catalytic efficiency of F96A was significantly less than that of the wild-type enzyme. Comparison of the crystal structures of the mutants F96Y (Figure 2A) and F96A (Figure 2B) with that of the PfTIM WT (Figure S4A) showed that there was no change in the conformation of any of the active-site residues. However, the water network observed for the mutant F96S (Figure S4B)[28] was not observed in F96Y. A notable feature of the mutant F96Y was the "*trans*" conformation of the Tyr96 side chain with $\chi_1 = 178^\circ$, even in the absence of any ligand and with loop-6 adopting an *open* state (Figure 2A and Table S5).

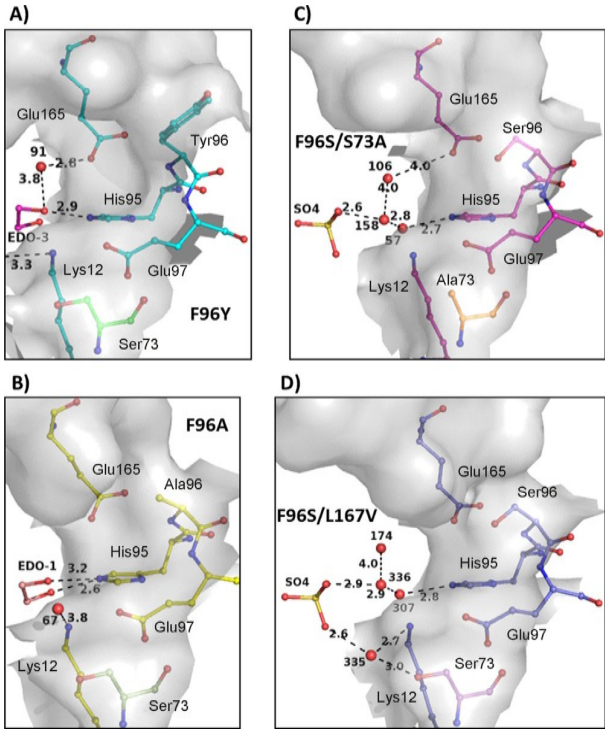


**Figure 2.** The active-site pocket with residues 96 and 73 (of the adjacent subunit), the catalytic residues K12, H95, E97, and E165, and the observed water (red spheres) and ligands [ethylene glycol (EDO) or sulfate ($SO_4^{2-}$), stick and ball]. Residues belonging to the adjacent subunits of the native dimer are shown in different colors. A) In F96Y, the extensive hydration observed for the F96S PfTIM mutant was absent, and the Tyr side chain was in a "*trans*" ($\chi_1 = 178^\circ$) conformation pointing away from the active site. B) F96A active site had an ethylene glycol unit hydrogen-bonded to His95. The C) F96S/S73A and D) F96S/L167V active site geometries were similar to that of the WT. Note that despite the presence of serine at positions 96 and 73 the water network connecting the two residues is absent in F96S/L167V, as was seen for F96S mutant.

### Probing the nature of the hydration of the active site with the double mutant F96S/S73A

The water networks observed in the cases of the F96S and F96H mutants are each anchored by residues 96 and 73 (of the adjacent subunit; Figure S4A and B, compare hydration of the active sites of PfTIM WT and F96S mutant).[26] Sequence conservation analysis highlights the preference for alanine at position 73, and PfTIM stands out in having serine at this position (Table 1). These observations raise the possibility that the two positions might be correlated and that maintaining a pair of polar and nonpolar residues at these positions might aid in catalysis. We argued that, if this assumption is correct, the double mutant F96S/S73A should rescue the loss of activity observed for F96S. Despite having a polar/nonpolar residue pair at positions 96 and 73, respectively, the mutant F96S/S73A showed both a turnover rate and an affinity ($k_{cat} \approx 46\ s^{-1}$, $K_m \approx 1.2$ mM) similar to those of the mutant F96S ($k_{cat} \approx 62\ s^{-1}$, $K_m \approx 2.2$ mM; Table 2). Comparison of the active site of the double mutant (Figure 2C) with those of yeast TIM (having S96 and A73 naturally, Figure S4C), PfTIM WT, and F96S (Figure S4A and B) confirmed no apparent change in conformation of any of the active-site residues. Contrary to our expectation, the double mutant F96S/S73A ($k_{cat}/K_m \approx 38\ mM^{-1}\ s^{-1}$) was found to be unsuccessful in rescuing the catalytic defect caused by F96S ($k_{cat}/K_m \approx 28\ mM^{-1}\ s^{-1}$;[28] Table 2). These observations do not support the presumed correlation of residues 96 and 73 in determining the catalytic efficiency of TIM.

### Exploring the mechanistic correlation and coevolution of residues 96 and 167

The spatial proximity of residue 96 to the loop-6 N-terminal hinge residue 167 is evident (Figure 1). Comparison of apo and ligand-bound forms of PfTIM shows that the movement in the residue 96 side chain is associated with changes in the backbone and/or side chain conformation of residue 167 (Figures 1B and S2C, Tables S5 and S6). Notably, residue 170, near the tip of loop-6, comes within van der Waals contact distance of the residue 96 side chain upon loop closure (Figure S2). The two residues 167 and 170 show limited variability in our curated TIM sequence dataset (Table 1 and Figure S3). In the dataset of 6610 unique bacterial and eukaryotic sequences, either Val or isoleucine was found in 97% of the sequences at position 167, whereas isoleucine was found in 99% of the sequen-


© 2016 Wiley-VCH Verlag GmbH & Co. KGaA, Weinheim

ces at position 170 (Table 1). Analysis of the amino acid occurrence at positions 96, 167, and 170 shows that although several triad combinations for the three amino acids are observed, the triads SVI (2779: bacteria; 676: eukaryote) and SII (2246: bacteria; 124: eukaryote) cover around 96% of bacterial sequences (5216 sequences) and 98% of eukaryotic sequences (819 sequences, Table S3). The triad observed for PfTIM (FLI) is a rare combination found only in four of the plasmodial sequences (Table S1 and S3) and in one bacterial sequence (Table S3).

The double mutant F96S/L167V (Figure 2D) was designed to improve understanding of the importance of the interaction between residue 96 and the loop-6 residues 167 and 170 and in an attempt to restore the activity of the mutant F96S. The mutant enzyme F96S/L167V showed improvement in both $k_{cat}$ (400 $s^{-1}$) and $K_m$ (1.0 mM) over F96S ($k_{cat}=62\ s^{-1}$; $K_m=2.2$ mM), though F96S/L167V was approximately ten times less active than PfTIM WT ($k_{cat}=4250\ s^{-1}$; $K_m=0.4$ mM, Table 2). The double mutant F96S/L167V turned out to be a "pseudo-revertant" with an increment of ≈14-fold in the specificity coefficient over that of the single-site mutant F96S. This observation was encouraging and persuaded us to examine further the correlation and coevolution of the residues at position 96 and the loop-6 residues 167 and 170.

## Conformational heterogeneity of residue 96 and its plausible role in catalysis

Residue 96 is a part of a short helix and has backbone dihedral angles of around $\varphi\approx-50^\circ$, $\psi\approx-37^\circ$ (Figure S2 and Table 3). Examination of the apo and holo forms of TIM (crystal structures available from 34 different organisms) reveals that the side chain of the residue 96 shows conformational heterogeneity (Tables 3 and S5, Figure S2). The side chain has been observed either in "*gauche*" ($\chi_1\approx45^\circ$) or in "*trans*" ($\chi_1\approx180^\circ$) conformations (Figure S2 and S5) when residue 96 is serine (in TIM structures from 32 different organisms, numbering as in PfTIM, Figure S2). In its "*gauche*" conformation, the S96 side chain points into the active-site cavity, and its backbone –NH group and side chain hydroxy $O_\gamma$ atom are at hydrogen-bonding distance from the catalytic base E165 side chain carboxylate oxygen atoms (Figure 2A, Figure S2A). In addition, the side chain is in van der Waals contact distance from the loop-6 hinge residue 167, and the hydroxy side chain $O_\gamma$ atom also makes a hydrogen bond with a conserved water molecule in the "*loop-open*" state of the enzyme (Figure S2A). In the "*trans*" conformation, the residue 96 side chain is flipped around 135° about the $C_\alpha$–$C_\beta$ bond, orienting the $O_\gamma$ atom of the serine side chain away from the active-site cavity (Figure S2). The "*trans*" conformation is stabilized by a new hydrogen bond between the S96 side chain and the residue 100 side chain, whereas the contact with E165 side chain is lost (Figure S5). The hydrogen bond between side chains of the residues 96 and 100 (positions as per PfTIM sequence) has been observed in several ligand-bound structures from different organisms (Figure S5A–D).

PfTIM is the only structurally characterized TIM with phenylalanine at position 96, and in this case an anion–π interaction between E165 and F96 (Figure S5G, based on the criteria for anion–π interactions described by Philip et al.[29]) replaces the E165···S96 hydrogen bond, characteristic of the "*gauche*" conformation. Also, in PfTIM, additional conformations of the F96 side chain with a range of $\chi_1=80^\circ$–$160^\circ$ ("*eclipsed*") have been observed in several ligand-bound structures (Figure S2C Figure S5E and Table S5). Given that residue 100 is a Lys in PfTIM and its side chain points away from the F96 aromatic ring, it is tempting to speculate that the absence of additional stabilization of F96 "*trans*" conformation is the reason for the observation of an intermediate "*eclipsed*" state of the F96 side chain (Table S5). Furthermore, because of the proximity of residue 96 (S/F) and the hinge residue 167 (V/I/L) side chains, the conformational transitions of residue 96 appear to be coupled to the conformational change of residue 167 (PfTIM PDB ID: 1LYX and 1O5X, Figures 1B and S5E, Table S5; *Mycobacterium tuberculosis* TIM-PDB ID: 3TAO, Figure S5F).

## Analysis of different structural states of TIM active sites—importance of residue 96

Comparison of the active site of TIM in the apo form [yeast TIM (ScTIM) PDB ID: 1YPI and *Leptospira interrogans* TIM (LiTIM) PDB ID: 4X22 (unpublished)] with that in the substrate-bound form [ScTIM PDB ID: 1NEY and LiTIM PDB ID: 4YMZ (unpublished)] highlights the conformational changes that occur concurrently with ligand binding and catalysis (Figures S2 and S6). The transition of the apo state to the catalytically competent state is accompanied by the following structural changes (Tables 3 and S6): 1) loop-6 closure and synchronized movement of loop-7 residues that help to anchor the substrate phosphate group (Figure S6),[12,15,16] 2) a change in the conformation of loop-6 N-terminal (P166-W168; Table S6) and C-terminal hinge residues (K174A176) and movement of the E165

**Table 3.** Backbone and side chain dihedral angles for residue 96 in *Saccharomyces cerevisiae* (*Sc*) and *L. interrogans* (*Li*) TIMs.

| Protein | PDB ID | Residue 96 | | | Ligand in active site | Loop-6 state | E165 state |
|---|---|---|---|---|---|---|---|
| | | $\varphi$ [°] | $\psi$ [°] | $\chi_1$ [°] | | | |
| ScTIM WT[a] | 1YPI | −50.7 | −37.3 | 45 (*gauche*) | – | *open* | swung-out |
| | 1NEY | −47.2 | −32.3 | 179.8 (*trans*) | DHAP | *closed* | swung-in |
| LiTIM WT[b] | 4X22 | −54.6 | −35.3 | 46.6 (*gauche*) | – | *open* | swung-out |
| | 4YMZ | −48.7 | −44.7 | 173.7 (*trans*) | DHAP | *closed* | swung-in |

[a] The corresponding conformation of the residues and loop-6 shown in Figures 3A and S2. [b] Data unpublished.


© 2016 Wiley-VCH Verlag GmbH & Co. KGaA, Weinheim

side chain from a "swung-out" (pointing away from active site) to a "swung-in" (pointing into the active site) conformation, and 3) a residue 96 side chain flip from "*gauche*" ($\chi_1 = 46^\circ$) to "*trans*" ($\chi_1 = 175^\circ$; Figure S2 and Table 3).

These structural changes close the substrate entry/exit route, place the substrate in proximity to the catalytic residues (Figure S6 A and B) and stabilize the loop-6 "*closed*" conformation for the duration of the catalytic cycle. If these three movements (Figure 3 A)—loop-6 ("*open*" and "*closed*"), residue 96 side chain ("*gauche*" and "*trans*"), and Glu165 ("swung-out" and "swung-in")—are considered as variables, different structural states for the TIM active site are possible (depicted as cartoon representations in Figure 3 B and C). Because of the direct link of residue 96 and the loop-6 residues 167 and 170, the triad combinations at these three residues will ensure optimal loop-6 dynamics and correlate the loop-6 movement to the conformational flip of E165. The correlated movement of residue 96 and 165 with loop-6 movement is an efficient way for the TIM to achieve catalytic competence upon substrate binding while promoting ligand binding in the apo form. The limited number of triad combinations (residues 96, 167, and 170) populating the dataset suggest that only a few combinations can carry out the function efficiently (Table S3).

In addition to the apo and the substrate-bound catalytically competent states depicted in Figure 3 A, in several structures of PfTIM a third state is also observed (Figures 1 B and S5 E). The characteristic of this ligand-bound state is loop-6 in "*closed*" form but E165 still in the catalytically incompetent "swung-out" conformation and residue 96 in a "*trans*" or "*eclipsed*" conformation (Figure S2 C and Table S5). In fact, several catalytically incompetent intermediary states between the apo and the catalytically competent states have been observed in crystal structures from different organisms (PDB IDs corresponding to the observed states are given in Figure 3); they suggest that TIM has several pathways by which to transit from the apo to the catalytically competent state and that the three depicted movements are the part of TIM active-site dynamics essential for catalysis.

## Discussion

The aim of this study was 1) to understand the part played by residue 96 in TIM catalysis and to investigate the possible reason behind its high degree of conservation, and 2) to understand the occurrence of Phe96 in PfTIM. Our work brings out the functional relevance of the conformational flexibility of residue 96 and its relation to ligand binding and catalysis in TIM.

### Lessons from the exception: PfTIM mutants and the assessment of the nature of hydration of the active site

PfTIM has a very rare residue—phenylalanine—at position 96 (in 98% of TIM sequences residue 96 is serine). Although an exception, PfTIM is still a functional isomerase and thus provides a unique opportunity to study the role of this residue. Previously, the kinetic and structural studies on the PfTIM mutants F96S, F96H, and F96W (Table S4)[28] had implicated residue 96 in regulation of the hydration of the active site, and a plausible correlation between residues 96 and 73 was suggested (Figure S4 B).[28] In this study, we replaced the nonpolar aromatic (Phe) residue 96 of PfTIM with a bulky polar aromatic (Tyr) and with a nonpolar small (Ala) residue. Catalytic rates of the F96 single mutants show the following order F96S ≈ F96H ≈ F96Y < F96A < F96W < PfTIM WT (Tables 2 and S4). Comparison of kinetic parameters obtained for all the single-site mutants clearly show that a polar residue (S, Y, or H) impedes PfTIM catalysis (Tables 2 and S4). F96A, with a nonpolar residue at position 96 ($k_{cat} \approx 11$ times less than the WT), was catalytically more efficient than F96S, whereas F96H and F96Y

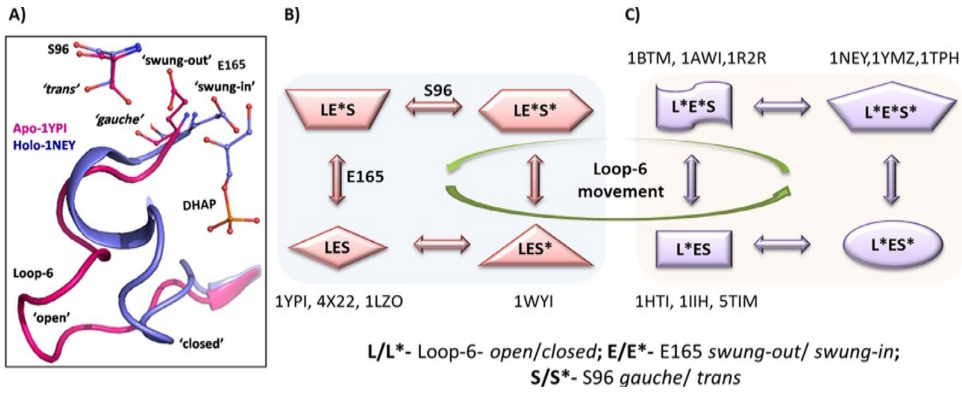


**Figure 3.** A) Crystallographically characterized apo (PDB ID: 1YPI) and substrate-bound catalytically competent holo (PDB ID: 1NEY) states of TIM. The transition from the apo state to the catalytically competent state involves movement of loop-6, the residue 96 side chain, and E165 and can give rise to different structural states of the TIM active site. These are pictorially represented in B) loop-6 "*closed*", and C) loop-6 "*open*" forms (corresponding PDB IDs of the states observed in crystal structures are indicated). The bottom state in C) with loop-6 "*open*", E165 "swung-out" conformation stabilized by residue 96 in "*gauche*" conformation is most feasible to allow ligand binding. The top-right-hand state in B) is the catalytically competent state with loop-6 "*closed*", E165 in "swung-in" conformation, and residue 96 side chain in its "*trans*" conformation. The conformational flip of residue 96 is a part of dynamic structural changes accompanying the catalytic cycle and is needed for achievement of catalytic competence.


© 2016 Wiley-VCH Verlag GmbH & Co. KGaA, Weinheim

(the mutant F96W), each with a bulky aromatic residue, retained ≈60% of the wild type activity and showed only marginal increases in $K_m$ (Tables 2 and S4). These observations could be partially explained by invoking the role of the residue 96 side chain in maintaining the hydration of the active site and the p$K_a$ of the active-site residues, as was suggested on the basis of structural studies of the chicken TIM mutant S96P (Table S4).[30,31] A change in the water network at the active site was suggested to be the cause of perturbations of electrostatic interactions involving the ammonium group of K12 and E165 and thus also the polarization of the substrate.[27] A more recent study established the presence of an extensive water network in the TIM active site, maintained by the residue at position 96 (when mutated to a polar residue—serine or histidine—in the PfTIM mutants F96S and F96H, respectively) and Ser73. This led to the suggestion that if the primary role of residue 96 is to maintain optimal hydration of the active site, the two positions might have coevolved for avoiding excessive hydration of the active site.[28] Contrary to our expectation, the mutants F96S and F96S/S73A showed comparable drops in $k_{cat}/K_m$ values (Table 2). This observation establishes that the mutation at position 73 does not offset the effect of F96S mutation, in turn suggesting that the plausible role of residue 96 in determining the rate of TIM catalysis remains unexplained by the hydration model.

### Phe96 in plasmodial TIM

Genes evolving under the selection for highly AT-rich genomes of plasmodia (≈70% AT content in the coding region)[32] are likely to show a mutational bias favoring mutations towards a more AT-rich codon (directional mutational pressure), and when non-synonymous, such directional mutations could lead to introduction of atypical amino acids in proteins.[33] This could arguably be the reason for Ser96 to Phe (codon UUU in all plasmodial TIM sequences) mutation in the plasmodial TIM sequences. Mutation of this residue back to the most favored residue at this position (F96S mutant) in the context of the PfTIM sequence drastically reduced catalytic efficiency. Coevolution of functionally correlated and critical residues is a strategy that could overcome the effect of missense mutations that cause functional defects. The reversal of the catalytic defect in the mutant F96S by the mutation F96S/L167V—"*pseudo-revertant*" (Table 2)—suggests that the positions 96 and 167 must have coevolved to maintain optimal dynamics of loop-6, which is critical for TIM catalysis. The epistatic effect of mutation at structurally correlated positions is responsible for the observation that substitution of a residue is contingent on the preceding mutation and that under purifying selection an unfavorable mutation gets fixed, when accompanied by a compensating mutation.[34,35] PfTIM turns out to be an example in which such a mutation of S96 to F and V167 to L might have been accepted because the reversion of either of the two residues will result in decoupling of the loop-6 dynamics and impede appropriate positioning of E165 in the active site, which in turn will cause catalytic impairment. The functional rationale for the existence of a high degree of conservation at position 96 and the identification of a coevolving cluster of residues (96, 167, and 170) emphasizes the utility of using the knowledge derived from large sequence datasets to probe structure–function relationships and to perform appropriate mutational studies to understand the selection pressure governing the evolution of enzyme sequences.

To obtain "clues to the essential dynamics" of an enzyme one often relies on the "availability of structures corresponding to different functional states" to gain insights into the reaction pathway.[36] In the cases in which protein dynamics are coupled to reaction coordinates or binding/release of the substrate/product, residues that are a part of this network are under strong evolutionary pressure and hence are observed to coevolve.[37] Thus, combining structural information with sequence conservation analysis can help to establish coevolving residues[38–41] and their role in enzyme catalysis,[42,43] structural stability, interprotein interactions, and macromolecular recognition.[44–48] In an interesting study of mutations at a highly conserved site in phosphoglycerate kinase (K219S), Wellner et al. suggest that "given enough time and variability in selection levels, even utterly conserved and functionally essential residues may change".[49]

### E165 and catalytic loop-6 conformational flexibility essential for TIM catalysis

The catalytic base E165 has been observed in two conformational states: "swung-in" and "swung-out". "Swung-in" is the catalytically competent conformation, with the side chain precisely poised for efficient proton abstraction. In this state, one of the E165 side chain carboxylate oxygen atoms ($O\varepsilon_1$) is positioned between the C1 and C2 carbon atoms of the substrate whereas, the other—$O\varepsilon_2$—remains at hydrogen bonding distance from the neutral imidazole ring of His95 (Figure S1).[50] In the "swung-out" conformation, the E165 side chain points away from the active site, and this conformation is stabilized through hydrogen bonds with the imidazole ring of H95 and the residue 96 backbone –NH group and by a hydrogen bond (Ser96)/anion–$\pi$ (Phe96) interaction with the residue 96 side chain hydroxy/aromatic ring (Figures 1A and S5G). The "swung-in" state will be repulsive for the approaching ligand, so the movement of E165 into and out of the active site aids substrate binding in the apo state, while allowing catalysis once the substrate is bound (Figures 3 and S6).

The 11-residue flexible loop (consensus sequence: "166-PVWAIGTGKTA-176", PfTIM numbering) present at the C terminus of the $\beta$-sheet-6 undergoes a hinged lid movement, shown to be critical in TIM catalysis.[13] The N-terminal (residues 166–169, PfTIM numbering) and C-terminal hinge (residues 174–176, PfTIM numbering) residues undergo a conformational change (Table S6).[13,51] Although the loop conformation changes are not ligand gated, the presence of ligand stabilizes the "*loop-closed*" conformation and affects the rate of loop opening.[52] T-jump relaxation studies and solid- and solution-state NMR studies established that loop-6 opening and closing rate constants are of the order of 100 μs.[23,53] Loop dynamics are partially rate-limiting for TIM-catalyzed isomerization of


© 2016 Wiley-VCH Verlag GmbH & Co. KGaA, Weinheim

DHAP and GAP.[23] Optimal conformational flexibility of loop-6 is a prerequisite for allowing opening and closing of the loop during catalytic turnover. Backbone hydrogen bonds, including the hinge residues and van der Waals contacts of its side chains, play a critical role in loop dynamics. The N- and C-terminal hinge mutants have been shown to be defective in catalysis and loop dynamics, and the N-terminal hinge sequence appears to be more critical for the loop-6 movement.[54–56]

Although it has been suggested that the conformation change of E165 and the change in backbone dihedral angles of the stretch 166–167 occurs prior to the proton-transfer step of catalysis,[57] NMR and MD simulation studies found no evidence for a direct physical coupling of loop dynamics and E165 positioning.[57,58] NMR studies exploring the effect of change in the loop-6 N-terminal hinge sequence PVW to PGG/GGG showed altered loop-6 dynamics in the mutants, emphasizing the role of "structural motional rigidity for focused freedom of the active site loop".[55] In a computational study on the chicken TIM mutant S96P, Dagget et al. remarked that the defect in catalysis in this mutant might be because of a change in the relative orientations of the key catalytic groups at positions 165 and 95.[59] In the light of these facts, the association of residue 96 side chain movement to the loop-6 tip residue 170 and the hinge residue 167 assumes importance for restructuring of the TIM active site upon substrate binding and attaining catalytic competence.

### Role of residue 96—coupling loop-6 dynamics to the conformational flip of E165

Upon ligand binding and loop-6 closure, I170 moves closer to the main body of the protein, and its side chain faces a steric clash with the "swung-in" conformation of E165 and the "*gauche*" conformation of S96 (Figure S2). Conformational flip in the residue 96 side chain ("*gauche*" to "*trans*") and its movement away from the active site releases this clash. A recent report advanced the proposal that the human TIM mutation I170V causes a defect in catalysis by altering the interaction with residue 96.[60] The movement of residue 96 is accompanied by a subtle conformational change in the backbone and side chain dihedral angles of residue 167 (Figures S2 and S5 E and F). The stretch of the N-terminal hinge residues of the active-site loop-6 (from residue 164 to 167) shows a conformational change, moving the E165 side chain by 2 Å and placing it closer to the substrate (Figure 3 A). Thus, residue 96 seems to be a pivot that couples the loop-6 closure to the appropriate movement of the loop-6 N-terminal hinge and placement of E165 side chain into the active-site pocket. According to this model, the transfer of the signal of loop-6 closure might largely depend on the combination of residues at positions 96, 167, and 170. The defect in ligand binding and catalysis in the F96S PfTIM mutant might arise from motional decoupling of the residue 96 and loop-6 N-terminal hinge residue 167. The proposal is strengthened by the finding that the same mutation in the background of L167V (double mutant F96S/L167V) resulted in a better catalyst (Table 2). The conservation pattern of the two positions suggests that a small residue is preferred for the function at position 96 when the N-terminal hinge position 167 is a valine or isoleucine residue (Tables S1 and S3). F96W was found to be catalytically slightly better than F96A, thus supporting the view that a bulkier residue is favored when residue 167 is a leucine (as in PfTIM) as opposed to a valine residue (most frequent residue at position 167). Packing constraints have been shown to restrict the loop-6 N terminus hinge sequence,[55] and our results support the view that the limited variability of the loop-6 N-terminal hinge residue 167 is probably driven by a need to conserve the dynamic requirements of the catalytic residue E165 and coupling the side chain movement of residue 96 to the loop-6 N-terminal hinge.

Recently, Samanta et al. have proposed an alternative pathway for the proton-transfer cycle in the TIM mechanism, involving reorientation of the His95 side chain during catalysis. The authors suggest that, instead of adopting an energetically unfavorable imidazolate form, the protonated His95 side chain flips to exchange a proton with the deprotonated E97 side chain.[8] The residue 96 side chain in its "*gauche*" conformation is likely to hinder the ring flip motion of H95 because the side chains of the two residue are in van der Waals contact (Figures 1 A and S5 G). Whereas the "*gauche*" conformation of residue 96 stabilizes the "swung-out" conformations of E165, its "*trans*" conformation is likely to be favorable for this ring flip of H95 during catalysis.

## Conclusions

The availability of a large number of protein sequences from diverse organisms allowed us to identify the positions around the active site (96, 167, and 170) of TIM that show limited sequence variability and appear to have coevolved, conserving the desired function. Residue 96 appears to correlate the loop-6 movement to the positioning of E165 into the catalytically competent conformation, thus playing an important role in making TIM a "perfect"[61] enzyme. Our results support the view that although residue 96 might influence the water network, it is also crucial in maintaining the loop-6 dynamics through its steric interactions with loop-6 residues 167 and 170 and precise positioning of the catalytic base E165. We have put forth an argument based on a comparative analysis of the crystallographically characterized states of TIM in its apo and the ligand-bound structures for the concomitant movement of loop-6, a residue 96 side chain conformation flip from "*gauche*" to "*trans*", and a transition of E165 from its inactive "swung-out" to the catalytically competent "swung-in" conformation. Our findings emphasize the importance of subtle motions related to the noncatalytic active-site residue 96 having a significant effect on catalysis. This opens the window for further investigation of the TIM mechanism by NMR and molecular dynamics with inclusion of residue 96.

## Experimental Section

**Dataset preparation and sequence conservation analysis**: A sequence search performed with use of "triosephosphate isomerase" as the search term yielded 14224 sequences (both reviewed and


© 2016 Wiley-VCH Verlag GmbH & Co. KGaA, Weinheim

unreviewed sequences) from the UniProt database. Because unreviewed sequences were also included in this analysis, the dataset was curated before multiple sequence alignment was performed. The sequences were divided into three subsets: 1) bacterial (9363 sequences), 2) eukaryotic (4309 sequences), and 3) archaeal (552 sequences). The following criteria were applied to each of the datasets: all of the entries with the words "fragment", "putative", "hypothetical", "unclassified", "uncultured", "unidentified", or "uncharacterized" and those that did not have the identifier EC 5.3.1.1 were excluded. When there were duplicates of a sequence (any identical sequences, with the same length, irrespective of the species), only one was retained, and sequences with one or more unassigned amino acid residues (denoted by X) were excluded, after which the length distribution of the sequences was obtained. A reasonable length cut-off around the median of distribution was applied (220–280 aa for bacteria, 230–330 aa for eukaryotes, 214–233 aa for archaea) such that all the sequences that were shorter or longer than the cut-off length were excluded. This was done in order to avoid anomalies during alignment, introduced as a result of large insertions or deletions in some exceptional sequences. Multiple sequence alignment was performed with the Clustal Omega tool.[62] Alignment of the three datasets was performed separately with use of the *Escherichia coli* TIM sequence for the bacterial dataset, the *P. falciparum* TIM sequence for the eukaryotic dataset, and the *Methanocaldococcus jannaschii* TIM sequence for the archaeal dataset. On the basis of the results of the alignment and current understanding of the residues important for catalysis and oligomerization, specific residue conservation criteria was applied for final curation of the datasets. For bacterial and eukaryotic datasets, sequences showing 100% conservation for the 10 residues K12, T75, H95, E97, C126, E165, P166, G209, G210, and G228 were retained for further analysis (numbering as in PfTIM). For the archaeal dataset, 100% conservation criteria included the residues equivalent to K12, T75, H95, E97, C126, E165, and P166 of PfTIM (SwissProt ID: Q07412). The final numbers of sequences in each of the dataset are provided in Table S2. By use of the multiply aligned dataset, the percentage similarities of all pairs of sequences in the dataset were computed. The pairwise minimum percentage sequence identities were seen to be 18% for the bacterial dataset, 23% for the eukaryotic dataset, and 26% for the archaeal dataset, whereas the maximum sequence identities were up to 100% in all the three cases. Separately, the 34 TIM sequences for which X-ray crystal structures are known, including bacterial, eukaryotic, and archaeal sequences, were aligned by using PfTIM as the template (with Clustal Omega), and a partial alignment of the sequences is shown for the region around residue 96 and loop-6 (figure prepared with ESPript 3.0—http://espript.ibcp.fr;[63] Figure S3).

**Cloning, expression, and purification of the mutants**: Each mutant gene was generated from the wild type *Plasmodium falciparum* triosephosphate isomerase gene by use of the single-primer method of site-directed mutagenesis[64] [oligonucleotides listed in Table S9 (New England Biolabs)]. The site of mutation and the change in codon are indicated as bold and underlined text. In all four mutants, due to the absence of a restriction endonuclease site at the desired position of mutation, a two-step process was followed: step 1, generating an intermediate clone to introduce the restriction site of EcoRV at the desired position of mutation, and step 2, taking the intermediate clone as template and generating the mutant clones F96Y, F96A, F96S/S73A, and F96S/L167V, along with the removal of the restriction site of EcoRV. An already available clone for the single mutant F96S was used as the template for the two double mutants F96S/S73A and F96S/L167V.[28] Mutant proteins were over-expressed in the AA200 *E. coli* strain, a null mutant of the host TIM gene,[65] and were purified as described previously.[28] Protein purity was checked by SDS-PAGE (12%; Figure S7), and mutation was confirmed by matching the expected mass with the derived masses obtained with use of the deconvolution module of the "Data Analysis 4.1" software (Bruker Daltonics). Electrospray ionization mass spectra were recorded with a MaXis impact Q-TOF instrument (Bruker Daltonics) coupled to an Agilent 1200 series online HPLC (Figures S9A and B, S10A and B). Final protein concentration was determined by use of the absorbance at 280 nm and Bradford's protein estimation assay with BSA as a standard.[66]

**Crystallization, data collection, processing, and structure refinement**: The mutant proteins were concentrated to about 10 mg mL$^{-1}$, and diffraction quality crystals were obtained by the hanging drop method within 10 to 14 days under the conditions reported in Table S10. Each hanging drop contained protein (3 μL) and the crystallization cocktail (3 μL) and was left to equilibrate with the crystallization cocktail (500 μL) as reservoir buffer. Diffraction data were collected with a Bruker AXS Microstar or Rigaku rotating anode generator and MAR Research image plate detector system, and ethylene glycol (15 to 20%) was used as cryoprotectant. Data were processed with iMOSFLM[68] and SCALA,[69–70] from the CCP4i suite of programs.[71–72] Crystals obtained for F96Y, F96A, and F96S/S73A belonged to the $P2_1$ space group, whereas that for F96S/L167V belonged to $P2_122_1$. The mutant structures were solved with the molecular replacement program PHASER 2.5.0[73] from the CCP4 package. The mutated residues, loop-6 residues, water molecules, and ligand were deleted from the MR and were added after few rounds of refinement on the basis of $2F_o-F_c$ and $F_o-F_c$ difference density maps contoured at 1 $\sigma$ and 3 $\sigma$, respectively (Figure S9C and D and Figure S10C and D). Refinement of the structures was carried out with REFMAC (version 5.5.0109).[74] Model building was performed with COOT v0.7.2.1,[75] and superposition of structures was done by the secondary superposition matching method in COOT.[76] The data collection and processing statistics and parameters after a final round of model building and refinement are provided in Tables S7 and S8. All images showing structural details were prepared with Pymol version 1.2r1.[76] After acceptable ranges of $R_{work}$ and $R_{free}$ (Table S8) had been achieved with final model building and refinement, the overall RMSD for structure superposition of the mutants with PfTIM WT was less than 1 Å, thus indicating that the overall structure was not perturbed due to the mutations introduced, and the RMSD for superimposition of the two subunits (subunits A and B of the same mutant) of the asymmetric unit was less than 1 Å (Table S11). All the mutant structures were obtained in their apo forms with loop-6 in its "*open*" conformation. In the absence of any specific crystal contacts with adjacent molecules, the loop-6 tip residues showed varying degrees of disorder in the side chain and in the backbone atoms corresponding to the loop-6 tip residues (Table S11).

**Enzyme activity**: With use of a continuous assay system, the activities of the mutant PfTIM WT and mutant enzymes were determined at 25 °C. Conversion from glyceraldehyde-3-phosphate (GAP) to dihydroxyacetone phosphate (DHAP) was monitored by the method of Plaut and Knowles.[67] For each of the mutants, the assay was repeated at least thrice and was found to be reproducible. Figure S8 shows an overlay of the Michaelis–Menten plots obtained with the average values from triplicates for each substrate concentration for the four PfTIM mutants. The values for the kinetic parameters ($K_m$, $k_{cat}$) and the associated errors were determined by fitting the initial velocity data (in triplicate) to the Michaelis–Menten equation with


© 2016 Wiley-VCH Verlag GmbH & Co. KGaA, Weinheim

Graphpad Prism (Version 5 for Windows, Graphpad software, San Diego, California, USA, www.graphpad.com; Figure S8 and Table 2).

## Acknowledgements

*The authors thank Sunitha Prakash for acquiring the protein mass spectra. Research on TIM was supported by a program grant from the Department of Biotechnology (India). X-ray diffraction and mass spectrometry facilities at the department were supported by program grants from the Department of Science and Technology and the Department of Biotechnology (India). V.P. and M.S. acknowledge IISc, Bangalore, and CSIR, New Delhi, India, for financial support. N.V.J. acknowledges the Ministry of Environment and Forests, Govt. of India, Dept. of Biotechnology, Govt. of India and IISc, Bangalore for partial financial support.*

**Keywords:** enzyme catalysis · isomerization · sequence conservation · structure–activity relationships · triosephosphate isomerase

[1] S. J. Putman, A. F. Coulson, I. R. Farley, B. Riddleston, J. R. Knowles, *Biochem. J.* **1972**, *129*, 301–310.
[2] A. Hall, J. R. Knowles, *Biochemistry* **1975**, *14*, 4348–4353.
[3] B. G. Miller, R. Wolfenden, *Annu. Rev. Biochem.* **2002**, *71*, 847–885.
[4] S. V. Rieder, I. A. Rose, *J. Biol. Chem.* **1959**, *234*, 1007–1010.
[5] J. R. Knowles, *Nature* **1991**, *350*, 121–124.
[6] E. A. Komives, L. C. Chang, E. Lolis, R. F. Tilton, G. A. Petsko, J. R. Knowles, *Biochemistry* **1991**, *30*, 3011–3019.
[7] E. B. Nickbarg, R. C. Davenport, G. A. Petsko, J. R. Knowles, *Biochemistry* **1988**, *27*, 5948–5960.
[8] M. Samanta, M. R. Murthy, H. Balaram, P. Balaram, *ChemBioChem* **2011**, *12*, 1886–1896.
[9] P. J. Lodi, L. C. Chang, J. R. Knowles, E. A. Komives, *Biochemistry* **1994**, *33*, 2809–2814.
[10] M. K. Go, T. L. Amyes, J. P. Richard, *J. Am. Chem. Soc.* **2010**, *132*, 13525–13532.
[11] M. K. Go, A. Koudelka, T. L. Amyes, J. P. Richard, *Biochemistry* **2010**, *49*, 5377–5389.
[12] G. Jogl, S. Rozovsky, A. E. McDermott, L. Tong, *Proc. Natl. Acad. Sci. USA* **2003**, *100*, 50–55.
[13] D. Joseph, G. A. Petsko, M. Karplus, *Science* **1990**, *249*, 1425–1428.
[14] D. L. Pompliano, A. Peyman, J. R. Knowles, *Biochemistry* **1990**, *29*, 3186–3194.
[15] X. Zhai, T. L. Amyes, R. K. Wierenga, J. P. Loria, J. P. Richard, *Biochemistry* **2013**, *52*, 5928–5940.
[16] M. G. Casteleijn, M. Alahuhta, K. Groebel, I. El-Sayed, K. Augustyns, A. M. Lambeir, P. Neubauer, R. K. Wierenga, *Biochemistry* **2006**, *45*, 15483–15494.
[17] E. Lolis, G. A. Petsko, *Biochemistry* **1990**, *29*, 6619–6625.
[18] E. Lolis, G. A. Petsko, *Annu. Rev. Biochem.* **1990**, *59*, 597–630.
[19] T. L. Amyes, J. P. Richard, *Biochemistry* **2007**, *46*, 5841–5854.
[20] Q. Cui, M. Karplus, *Adv. Protein Chem.* **2003**, *66*, 315–372.
[21] J. P. Richard, *Biochemistry* **1991**, *30*, 4581–4585.
[22] J. P. Richard, *Biochem. Soc. Trans.* **1993**, *21*, 549–553.
[23] S. Rozovsky, G. Jogl, L. Tong, A. E. McDermott, *J. Mol. Biol.* **2001**, *310*, 271–280.
[24] S. Rozovsky, A. E. McDermott, *J. Mol. Biol.* **2001**, *310*, 259–270.
[25] R. Arya, M. R. Lalloz, A. J. Bellingham, D. M. Layton, *Hum. Mutat.* **1997**, *10*, 290–294.
[26] T. C. Alber, R. C. Davenport, Jr., D. A. Giammona, E. Lolis, G. A. Petsko, D. Ringe, *Cold Spring Harbor Symp. Quant. Biol.* **1987**, *52*, 603–613.
[27] Z. Zhang, E. A. Komives, S. Sugio, S. C. Blacklow, N. Narayana, N. H. Xuong, A. M. Stock, G. A. Petsko, D. Ringe, *Biochemistry* **1999**, *38*, 4389–4397.
[28] P. Gayathri, M. Banerjee, A. Vijayalakshmi, H. Balaram, P. Balaram, M. R. N. Murthy, *Acta Crystallogr. Sect. D Biol. Crystallogr.* **2009**, *65*, 847–857.
[29] V. Philip, J. Harris, R. Adams, D. Nguyen, J. Spiers, J. Baudry, E. E. Howell, R. J. Hinde, *Biochemistry* **2011**, *50*, 2939–2950.
[30] S. C. Blacklow, J. R. Knowles, *Biochemistry* **1990**, *29*, 4099–4108.
[31] S. C. Blacklow, K. D. Liu, J. R. Knowles, *Biochemistry* **1991**, *30*, 8470–8476.
[32] M. J. Gardner, N. Hall, E. Fung, O. White, M. Berriman, R. W. Hyman, J. M. Carlton, A. Pain, K. E. Nelson, S. Bowman, I. T. Paulsen, K. James, J. A. Eisen, K. Rutherford, S. L. Salzberg, A. Craig, S. Kyes, M. S. Chan, V. Nene, S. J. Shallom, et al., *Nature* **2002**, *419*, 498–511.
[33] N. Sueoka, *Proc. Natl. Acad. Sci. USA* **1988**, *85*, 2653–2657.
[34] P. Shah, D. M. McCandlish, J. B. Plotkin, *Proc. Natl. Acad. Sci. USA* **2015**, *112*, E3226–3235.
[35] M. Lunzer, G. B. Golding, A. M. Dean, *PLoS Genet.* **2010**, *6*, e1001162.
[36] M. Karplus, J. Kuriyan, *Proc. Natl. Acad. Sci. USA* **2005**, *102*, 6679–6685.
[37] J. P. Klinman, A. Kohen, *J. Biol. Chem.* **2014**, *289*, 30205–30212.
[38] S. W. Lockless, R. Ranganathan, *Science* **1999**, *286*, 295–299.
[39] A. I. Shulman, C. Larson, D. J. Mangelsdorf, R. Ranganathan, *Cell* **2004**, *116*, 417–429.
[40] Z. O. Wang, D. D. Pollock, *Methods Enzymol.* **2005**, *395*, 779–790.
[41] D. de Juan, F. Pazos, A. Valencia, *Nat. Rev. Genet.* **2013**, *14*, 249–261.
[42] S. C. Kamerlin, A. Warshel, *Proteins Struct. Funct. Bioinf.* **2010**, *78*, 1339–1375.
[43] J. P. Klinman, *Acc. Chem. Res.* **2015**, *48*, 449–456.
[44] M. Socolich, S. W. Lockless, W. P. Russ, H. Lee, K. H. Gardner, R. Ranganathan, *Nature* **2005**, *437*, 512–518.
[45] N. Halabi, O. Rivoire, S. Leibler, R. Ranganathan, *Cell* **2009**, *138*, 774–786.
[46] T. A. McMurrough, R. J. Dickson, S. M. Thibert, G. B. Gloor, D. R. Edgell, *Proc. Natl. Acad. Sci. USA* **2014**, *111*, E2376–2383.
[47] R. A. Estabrook, J. Luo, M. M. Purdy, V. Sharma, P. Weakliem, T. C. Bruice, N. O. Reich, *Proc. Natl. Acad. Sci. USA* **2005**, *102*, 994–999.
[48] Y. Lee, J. Mick, C. Furdui, L. J. Beamer, *PLoS One* **2012**, *7*, e38114.
[49] A. Wellner, M. Raitses Gurevich, D. S. Tawfik, *PLoS Genet.* **2013**, *9*, e1003665.
[50] R. C. Davenport, P. A. Bash, B. A. Seaton, M. Karplus, G. A. Petsko, D. Ringe, *Biochemistry* **1991**, *30*, 5821–5826.
[51] E. Lolis, T. Alber, R. C. Davenport, D. Rose, F. C. Hartman, G. A. Petsko, *Biochemistry* **1990**, *29*, 6609–6618.
[52] J. C. Williams, A. E. McDermott, *Biochemistry* **1995**, *34*, 8309–8319.
[53] R. Desamero, S. Rozovsky, N. Zhadin, A. McDermott, R. Callender, *Biochemistry* **2003**, *42*, 2941–2951.
[54] J. Sun, N. S. Sampson, *Biochemistry* **1999**, *38*, 11474–11481.
[55] J. G. Kempf, J. Y. Jung, C. Ragain, N. S. Sampson, J. P. Loria, *J. Mol. Biol.* **2007**, *368*, 131–149.
[56] J. Xiang, J. Y. Jung, N. S. Sampson, *Biochemistry* **2004**, *43*, 11436–11445.
[57] N. S. Sampson, J. R. Knowles, *Biochemistry* **1992**, *31*, 8488–8494.
[58] P. Derreumaux, T. Schlick, *Biophys. J.* **1998**, *74*, 72–81.
[59] V. Daggett, F. Brown, P. Kollman, *J. Am. Chem. Soc.* **1989**, *111*, 8247–8256.
[60] B. P. Roland, C. G. Amrich, C. J. Kammerer, K. A. Stuchul, S. B. Larsen, S. Rode, A. A. Aslam, A. Heroux, R. Wetzel, A. P. VanDemark, M. J. Palladino, *Biochim. Biophys. Acta Mol. Basis Dis.* **2015**, *1852*, 61–69.
[61] W. J. Albery, J. R. Knowles, *Biochemistry* **1976**, *15*, 5631–5640.
[62] F. Sievers, A. Wilm, D. Dineen, T. J. Gibson, K. Karplus, W. Li, R. Lopez, H. McWilliam, M. Remmert, J. Soding, J. D. Thompson, D. G. Higgins, *Mol. Syst. Biol.* **2011**, *7*, 539.
[63] X. Robert, P. Gouet, *Nucleic Acids Res.* **2014**, *42*, W320–324.
[64] A. R. Shenoy, S. S. Visweswariah, *Anal. Biochem.* **2003**, *319*, 335–336.
[65] A. Anderson, R. A. Cooper, *J. Gen. Microbiol.* **1970**, *62*, 329–334.
[66] M. M. Bradford, *Anal. Biochem.* **1976**, *72*, 248–254.
[67] B. Plaut, J. R. Knowles, *Biochem. J.* **1972**, *129*, 311–320.
[68] A. G. W. Leslie, H. R. Powell, *NATO Sci. Ser. II* **2007**, *245*, 41–51.
[69] S. French, K. Wilson, *Acta Crystallogr. Sect. A Cryst. Phys. Diffr. Theor. Gen. Crystallogr.* **1978**, *34*, 517–525.
[70] P. Evans, *Acta Crystallogr. Sect. D Biol. Crystallogr.* **2006**, *62*, 72–82.
[71] E. Potterton, P. Briggs, M. Turkenburg, E. Dodson, *Acta Crystallogr. Sect. D Biol. Crystallogr.* **2003**, *59*, 1131–1137.


© 2016 Wiley-VCH Verlag GmbH & Co. KGaA, Weinheim

[72] M. D. Winn, C. C. Ballard, K. D. Cowtan, E. J. Dodson, P. Emsley, P. R. Evans, R. M. Keegan, E. B. Krissinel, A. G. Leslie, A. McCoy, S. J. McNicholas, G. N. Murshudov, N. S. Pannu, E. A. Potterton, H. R. Powell, R. J. Read, A. Vagin, K. S. Wilson, *Acta Crystallogr. Sect. D Biol. Crystallogr.* **2011**, *67*, 235 – 242.
[73] A. J. McCoy, R. W. Grosse-Kunstleve, P. D. Adams, M. D. Winn, L. C. Storoni, R. J. Read, *J. Appl. Crystallogr.* **2007**, *40*, 658 – 674.
[74] G. N. Murshudov, A. A. Vagin, E. J. Dodson, *Acta Crystallogr. Sect. D Biol. Crystallogr.* **1997**, *53*, 240 – 255.
[75] P. Emsley, B. Lohkamp, W. G. Scott, K. Cowtan, *Acta Crystallogr. Sect. D Biol. Crystallogr.* **2010**, *66*, 486 – 501.
[76] W. L. DeLano, 1.2r1 ed., Delano Scientific, San Carlos, CA, USA, **2002**.

Manuscript received: October 13, 2015
Accepted article published: January 14, 2016
Final article published: February 29, 2016


© 2016 Wiley-VCH Verlag GmbH & Co. KGaA, Weinheim